Formation of nonreciprocal bands in magnetized diatomic plasmonic chains

C. W. Ling,[1] Jin Wang,[2] and Kin Hung Fung[1,*]
[1]*Department of Applied Physics, Hong Kong Polytechnic University, Hong Kong*
[2]*Department of Physics, Southeast University, Nanjing 211189, China*
(Received 9 August 2015; revised manuscript received 29 September 2015; published 26 October 2015)

We show that nonreciprocal bands can be formed in a magnetized periodic chain of spherical plasmonic particles with two particles per unit cell. Simplified forms of symmetry operators in dipole approximations are used to demonstrate explicitly the relation between spectral nonreciprocity and broken spatial-temporal symmetries. Due to hybridization among plasmon modes and free-photon modes, strong spectral nonreciprocity appears in the region slightly below the light line, where highly directed guiding of energy can be supported. The results may provide clear guidance on the design of one-way waveguides.

DOI: 10.1103/PhysRevB.92.165430 PACS number(s): 73.20.Mf, 78.67.Pt, 11.30.Qc

I. INTRODUCTION

Breaking Lorentz reciprocity [1,2] in optics has been of great interest to physicists for many decades. In recent years, the asymmetry in dispersion relation $\omega(-\mathbf{k}) \neq \omega(\mathbf{k})$ (i.e., spectral nonreciprocity) [3,4] has drawn a great deal of interest because of its possible topological nature [5] and potential applications such as on-chip optical isolators, unidirectional waveguides, and circulators [6–9]. Nonreciprocal bands predicted by topological band theory usually appear as surface modes attached to two-dimensional (2D) or three-dimensional (3D) bulk photonic systems. To make the device more compact, approaches based on symmetry breaking in waveguide structures usually suggest complex geometries such as helical structures [5,10–12].

Spectral reciprocity, $\omega(-\mathbf{k}) = \omega(\mathbf{k})$, can be protected by time-reversal symmetry ($\mathcal{T}$) and spatial symmetries such as inversion ($\mathcal{P}$) [3,4], in addition to the local symmetries in permittivity or permeability tensors ($\boldsymbol{\epsilon}^{\mathrm{T}} = \boldsymbol{\epsilon}$ or $\boldsymbol{\mu}^{\mathrm{T}} = \boldsymbol{\mu}$). It is easy to understand that $\mathcal{T}$ symmetry can be broken by external static magnetic field [5], while $\mathcal{P}$ symmetry can be broken by using asymmetric structures such as chiral structures [5,10–12] or a symmetrical structure under external magnetic field of specific orientation [13]. However, spectral reciprocity can also be protected by a combination of symmetries such as spatial-temporal symmetries, which add more complexities in the design of nonreciprocal waveguides.

In this paper, we use compact nonchiral magnetized plasmonic waveguides consisting of only spherical particles to demonstrate how spectral reciprocity can be protected by a rotation-time-reversal ($\mathcal{RT}$) symmetry (i.e., time reverse followed by rotation of 180° about propagation x axis). In the $\mathcal{RT}$-symmetry-broken case, we show that asymmetric dispersion relation can be supported. By coupling the hybridized bands with light lines, this simple system further supports one-way wave propagation and energy transmission within a finite range of frequencies.

II. MODEL AND METHODS

We start by considering a magnetized diatomic system as shown in Fig. 1. The chain contains two types of metallic nanoparticles with different sizes, namely particle A and B, with the same dielectric constant $\boldsymbol{\epsilon}(\omega)/\epsilon_0$. The two nanoparticles formed "atoms" of a unit cell, and hence it is regarded as a dimer chain. As long as the nanoparticles are not too close together, the electromagnetic responses of the nanoparticles can be modeled by electric dipoles [14]. We denote the dipole moment of the nanoparticle in the nth unit cell as $\mathbf{p}_{n;\sigma}$, where $\sigma = A$ or B for type A and B particles, respectively. These dipole moments satisfy a set of self-consistent equations, known as the coupled dipole equations [14–16],

$$\sum_{m,\sigma'} \left(\boldsymbol{\alpha}_{\sigma}^{-1}\delta_{nm}\delta_{\sigma\sigma'} - \mathbf{G}_{nm\sigma\sigma'}\right)\mathbf{p}_{m;\sigma'} = \mathbf{E}_{n;\sigma}^{\mathrm{ext}}, \tag{1}$$

in which m runs from $-N$ to N, $\sigma' = A$ or B, δ_{nm} is the Kronecker delta function, and $\mathbf{E}_{n;\sigma}^{\mathrm{ext}}$ is the external driving field. We note that $\boldsymbol{\alpha}_{\sigma}$ is the quasistatic polarizability with radiation correction of nanoparticle σ, and $\mathbf{G}_{nm\sigma\sigma'}$ is interaction between dipoles $\mathbf{p}_{m;\sigma'}$ and $\mathbf{p}_{n;\sigma}$. Expressions are given in Appendix A 1 [see Eqs. (A1) and (A4)].

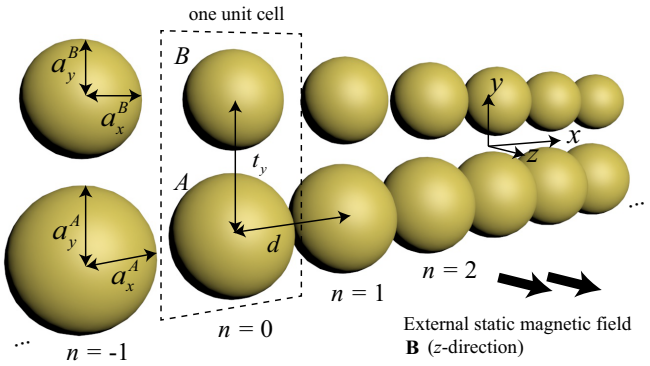

FIG. 1. (Color online) Geometry of a diatomic chain system. The chain contains two metallic nanoparticles in a unit cell, denoted by A and B. They can be elliptical or spherical, dependent on the values of semimajor axis a_x^{σ} and semiminor axis a_y^{σ}, where $\sigma = A$ or B. In the case of spherical, $a_x^{\sigma} = a_y^{\sigma}$. A and B are separated by distance t_y. External static magnetic field **B** is applied in z direction. Length of a unit cell is d. The chain breaks time-reversal ($\mathcal{T}$), inversion ($\mathcal{P}$), and rotation-time-reversal ($\mathcal{RT}$) symmetry. $\mathcal{RT}$ is defined by time reversal followed by rotating the structure about the chain axis by 180°.

*khfung@polyu.edu.hk

We first consider the case without external driving field ($\mathbf{E}^{\text{ext}}_{n;\sigma} = 0$) and $N \to \infty$. Since the system is spatially periodic, by Bloch's theorem we can write $\mathbf{p}_{m;\sigma} = \mathbf{p}_{k;\sigma} e^{ikmd}$, where k is a wave vector. This simplifies Eq. (1) into a 6×6 matrix form [see Eq. (A3)]:

$$\mathbf{M}_k(\omega)\begin{bmatrix}\mathbf{p}_{k;A}\\ \mathbf{p}_{k;B}\end{bmatrix} = 0, \tag{2}$$

where

$$\mathbf{M}_k(\omega) = \begin{bmatrix}\boldsymbol{\alpha}_A^{-1} & 0\\ 0 & \boldsymbol{\alpha}_B^{-1}\end{bmatrix} - \begin{bmatrix}\mathbf{G}_{kAA} & \mathbf{G}_{kAB}\\ \mathbf{G}_{kBA} & \mathbf{G}_{kBB}\end{bmatrix}. \tag{3}$$

In the above $\mathbf{G}_{k\sigma\sigma'} = \sum_m \mathbf{G}_{0m\sigma\sigma'} e^{ikmd}$ is the interaction between nanoparticles σ and σ' in k space. Instead of solving $\det \mathbf{M}_k(\omega) = 0$ to obtain the dispersion relation [10,14,17], we may apply a method similar to the eigenresponse theory to evaluate the dispersion relation [15,18]. We plot $1/|\lambda|$ as a function of k and ω, where $|\lambda| = |\lambda(k,\omega)|$ is the smallest absolute value of the eigenvalue of the matrix $\mathbf{M}_k(\omega)$. This quantity gives a huge value when there is resonance, and is plotted in Fig. 2(a). Note that the dynamic dipolar Green's function [10] is used, and an infinite series in the interaction up to $|m| = 120$.

III. FORMATION OF NONRECIPROCAL BANDS

In Fig. 2(a), we show the geometry and corresponding dispersion relation for the four in-plane modes in subpanels (i) and (ii). This case considers that nanoparticles are spherical with radius $a_x^A = 0.35d$ and $a_x^B = \sqrt[3]{0.5}a_x^A$, inner particle separation $t_y = 0.75d$, and plasma wavelength $\lambda_d \equiv c/(2\pi\omega_p) = 10d$, where ω_p and c are plasma frequency and light speed in vacuum. Cyclotron frequency $\omega_c = q|\mathbf{B}|/m = 0.005\omega_p$, in which $\mathbf{B}$, m, and q are external static magnetic field, electron mass, and electron charge. As $\omega_c \propto |\mathbf{B}|$, it is treated as a variable to indicate the magnitude of $\mathbf{B}$. Furthermore, for simplicity, a simple lossless Drude model is used [19], and bands related to $p^z_{k;\sigma}$, the z component of $\mathbf{p}_{k;\sigma}$, are not shown. This is because $\mathbf{B}$ is in the z direction, so $p^x_{k;\sigma}$ are coupled with $p^y_{k;\sigma}$ but not $p^z_{k;\sigma}$, hence the bands can be separated. Note that the two solid blue lines are light lines, the dispersion of free-photon modes. The region within the light lines is the light cone; the modes in the light cone are radiative and therefore not sustainable [10,20,21].

Figure 2(a) shows a case with nonreciprocal (asymmetric) bands. For comparison, using the same formalism, a case with reciprocal (symmetric) bands is shown in Fig. 2(b). This is a case where nanoparticles B and A are on the same axis, and the horizontal inner separation is $t_x = 0.425d'$, where d' is the length of the unit cell in (b). We set $d' = 2d$, twice that in (a); therefore the light cone in (b) is bigger than that in (a). Both (a) and (b) share the same nanoparticles A and B, cyclotron frequency ω_c, and plasma wavelength λ_d ($\lambda_p = 5d'$ in this case).

The nonreciprocal bands in Fig. 2(a), subpanel (ii), predict that only guided modes with positive group velocities are allowed within the range $\Delta\omega$. This results in one-way propagation behavior, which can be utilized as an isolator. Note that the operation frequency $\Delta\omega$ is relatively broad, for example, about 50 times wider than the structure suggested in Ref. [10]. The range of operation frequency is about $1 \times 10^{-4}\omega_p$ in Ref. [10], while we have about $5 \times 10^{-3}\omega_p$. The isolator also has a lower requirement on the external magnetic field, where cyclotron

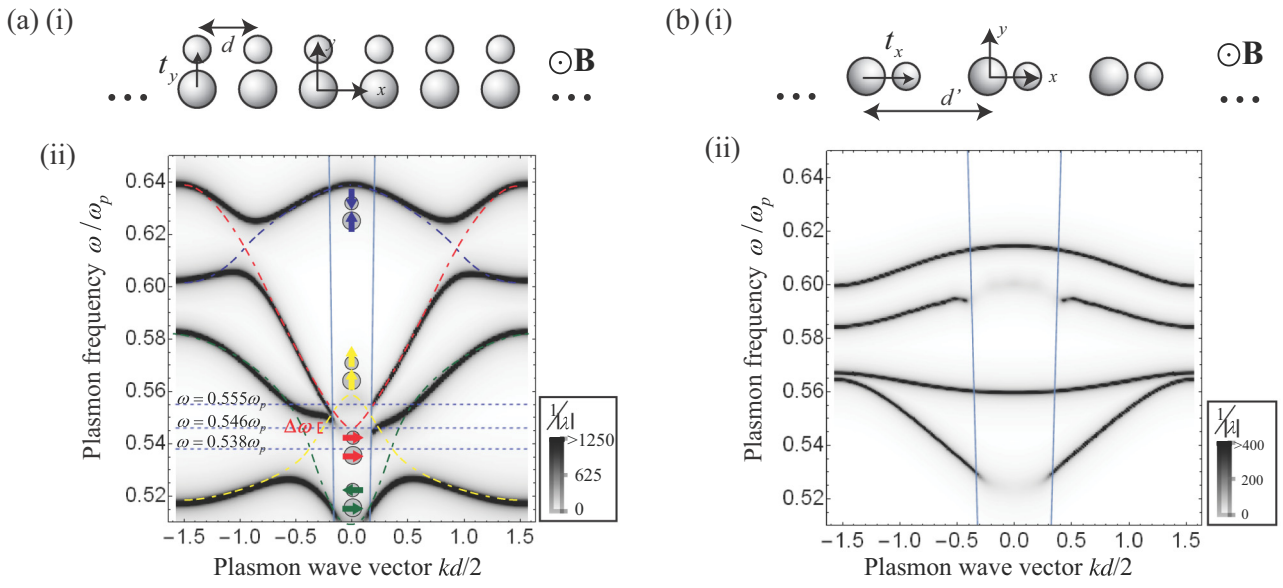

FIG. 2. (Color online) Dispersion relations for an infinitely long and magnetized diatomic chain system without $\mathcal{RT}$ symmetry (a) and with $\mathcal{RT}$ symmetry (b). Subpanel (i) is the chain geometry, while (ii) is the corresponding dispersion relation obtained by density plot of $1/|\lambda|$, where λ is the smallest eigenvalue of $\mathbf{M}_k(\omega)$ defined in Eq. (2). Panel (a), subpanel (ii), shows nonreciprocal bands [$\omega(k) \neq \omega(-k)$], while only reciprocal bands [$\omega(k) = \omega(-k)$] can be seen in panel (b), subpanel (ii). Bands related to the z component are separated and not shown here. The blue solid lines are dispersions of free-photon modes. Inner particle separation in (a) is $t_y = 0.75d$, and in (b) is $t_x = 0.425d'$, where $d' = 2d$. Furthermore, panel (a), subpanel (ii), can be understood as hybridization of 4 bands, which are schematically drawn with dashed lines for guidance. Each dashed line represents different oscillation modes at $k = 0$, which is labeled by arrows at the middle. $\Delta\omega$ is the range at which only one-way propagation modes are allowed.

frequency $\omega_c \sim 0.005\omega_p$ is about 10 times smaller than that used in Refs. [10,11], and about 100 times smaller than that in Ref. [22]. A higher resolution of the one-way region as well as the estimation of $\Delta\omega$ are discussed in Sec. V C.

We notice that the nonreciprocal bands in Fig. 2(a) are obtained by means of the simultaneous violation of certain symmetries, $\mathcal{P}$, $\mathcal{T}$, and $\mathcal{RT}$ symmetries, whereas the only breaking of $\mathcal{P}$ and $\mathcal{T}$ still makes the system reciprocal shown in Fig. 2(b). We will discuss the relation between reciprocity and related symmetries below.

A. Reciprocity protected by $\mathcal{P}$ and $\mathcal{T}$ symmetry

Given that $\mathbf{p}_{n;\sigma}(t) = \mathbf{p}_{k;\sigma}e^{iknd-i\omega t}$ is a solution of a system with frequency ω and wave vector k, the spatially inverted state will be $\mathcal{P}[\mathbf{p}_{n;\sigma}(t)] = \mathcal{P}(\mathbf{p}_{k;\sigma})e^{-iknd-i\omega t}$. $\mathcal{P}$ turns (x,y,z) into $(-x,-y,-z)$, flips the direction of vector quantities, but does not modify ω. If the system has $\mathcal{P}$ symmetry, the inverted state will also be the solution of the system. The factor $e^{-iknd-i\omega t}$ of the new solution means that it is a solution with frequency ω but wave vector $-k$. This tells us that we are always able to find a solution with frequency ω but wave vector $-k$ if the system has $\mathcal{P}$ symmetry, and thus the dispersion must be symmetric $[\omega(k) = \omega(-k)]$.

The time-reversed state is obtained by taking the complex conjugate of the frequency component (see Ref. [23], and also Appendix A 5),

$$\mathcal{T}[\mathbf{p}_{n;\sigma}(t)] = (\mathbf{p}_{k;\sigma}e^{iknd})^*e^{-i\omega t} = \mathbf{p}^*_{k;\sigma}e^{-iknd-i\omega t}. \tag{4}$$

This will be another solution if the system has $\mathcal{T}$ symmetry. Similarly, it is a solution with frequency ω but wave vector $-k$, as it has the factor $e^{-iknd-i\omega t}$. Using arguments as those in $\mathcal{P}$ symmetry, we know the bands are symmetric as long as there is $\mathcal{T}$ symmetry. We see that, from Fig. 3, the direction of external $\mathbf{B}$ will be flipped if $\mathcal{T}$ is operated on the system. Thus, the presence of external $\mathbf{B}$ breaks $\mathcal{T}$ symmetry, as the transformed one is not identical to the initial one.

Note that a lossy system will also break $\mathcal{T}$ symmetry. We assumed that the material is lossless, and the effect of radiation loss is compensated if we count the contributions from all nanoparticles in the infinite chain system [25]. So the $\mathcal{T}$ symmetry will be broken by external $\mathbf{B}$ only.

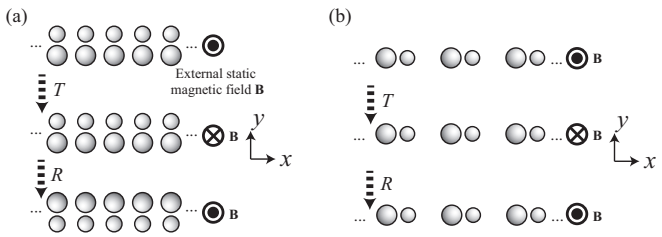

FIG. 3. $\mathcal{RT}$ acts on the diatomic chain systems shown in Fig. 2. $\mathcal{T}$ is time-reversal operation, which flips the direction of $\mathbf{B}$ when acting on the system. This can be understood as the motion of electrons being reversed [24]. $\mathcal{R}$ is π rotation about the x axis. It exchanges the positions of A and B and flips the direction of $\mathbf{B}$ in case (a), and only flips $\mathbf{B}$ in case (b). $\mathcal{RT}$ is the operation $\mathcal{T}$ followed by $\mathcal{R}$. For (a), as the final system is not identical to the initial one, the chain does not have $\mathcal{RT}$ symmetry. For (b), the final system is identical to the initial one, and the chain has $\mathcal{RT}$ symmetry.

B. Reciprocity protected by $\mathcal{RT}$ symmetry

$\mathcal{R}$ is the π-rotation operator, which rotates the system with 180° about the x axis. In the case of the diatomic chain system shown in Fig. 1, the direction of external $\mathbf{B}$ is flipped, and the positions of A and B are exchanged; see Fig. 3. $\mathcal{RT}$ is the operation $\mathcal{T}$ followed by $\mathcal{R}$. When $\mathcal{RT}$ acts on the solution, we have

$$\mathcal{RT}[\mathbf{p}_{n;\sigma}(t)] = \mathcal{R}(\mathbf{p}^*_{k;\sigma}e^{-iknd-i\omega t}) = \mathcal{R}(\mathbf{p}^*_{k;\sigma})e^{-iknd-i\omega t}. \tag{5}$$

Here we used the property that $\mathcal{R}$ is not related to position x and time $\mathcal{T}$. Again, if the system has $\mathcal{RT}$ symmetry, Eq. (5) will be a solution with frequency ω but wave vector $-k$. This shows that the bands are symmetric about k.

The matrix representation of $\mathcal{R}$ depends on system geometry. For the chain system shown in Fig. 2(a), $\mathcal{R}$ not only exchanges the positions of A and B, but also rotates the vector quantities when acting on the states. Denoting the 3×3 rotation matrix which rotates a vector about the x axis with 180° by $\mathbf{R} = \mathrm{diag}(1,-1,-1)$, then the $\mathcal{RT}$ transformed state is

$$\mathcal{RT}[\mathbf{p}_{n;\sigma}(t)] = \begin{bmatrix} 0 & \mathbf{R} \\ \mathbf{R} & 0 \end{bmatrix}\begin{bmatrix} \mathbf{p}^*_{k;A} \\ \mathbf{p}^*_{k;B} \end{bmatrix}e^{-iknd-i\omega t}. \tag{6a}$$

For the chain system shown in Fig. 2(b), $\mathcal{R}$ does not exchange positions of A and B, so the $\mathcal{RT}$ transformed state is

$$\mathcal{RT}[\mathbf{p}_{n;\sigma}(t)] = \begin{bmatrix} \mathbf{R} & 0 \\ 0 & \mathbf{R} \end{bmatrix}\begin{bmatrix} \mathbf{p}^*_{k;A} \\ \mathbf{p}^*_{k;B} \end{bmatrix}e^{-iknd-i\omega t}. \tag{6b}$$

For the system of Fig. 2(a), the external $\mathbf{B}$ breaks the $\mathcal{T}$ symmetry, and simultaneously the nonidentical nanoparticles A and B break the $\mathcal{P}$ and $\mathcal{RT}$ symmetry; see Fig. 3. The nonreciprocal band could then be obtained as shown in Fig. 2(a), subpanel (ii). In contrast, when $\mathcal{RT}$ acts on the system shown in Fig. 2(b), $\mathbf{B}$ is flipped twice and remains unchanged. Meanwhile, particles A and B are on the x axis, $\mathcal{R}$ would not modify their positions, and thus the transformed system is identical to the nontransformed one, which means it has $\mathcal{RT}$ symmetry. More details in quasistatic approximation is provided in Appendix A 6. We get the reciprocal dispersion relation in Fig. 2(b), subpanel (ii).

Therefore, in order to obtain nonreciprocal bands in a 1D magnetized chain system, it is essential to break all related symmetries, including $\mathcal{P}$, $\mathcal{T}$, and $\mathcal{RT}$ symmetries. It should be noted that the $\mathcal{R}$ operator above can be replaced by reflection-in-y in our example. Similarity between π-rotation and reflection-in-y is discussed in Appendix A 7.

IV. SYMMETRY OPERATORS ON DIATOMIC CHAIN SYSTEM

A system is said to have Θ symmetry if it is invariant under transformation, $\Theta\mathbf{M}_k(\omega)\Theta^{-1} = \mathbf{M}_k(\omega)$. Here we show explicitly that the $\mathcal{T}$ and $\mathcal{RT}$ operate on the coupled dipole equation $\mathbf{M}_k(\omega)$. For simplicity, we consider the system shown in Fig. 1, employ the quasistatic dipolar Green's function, use a simple lossless Drude model, and neglect the radiation term in polarizability.

A. Coupled dipole equation in quasistatic limit

Quasistatic expressions are obtained by taking free-space wave vector $k_0 \to 0$, so the polarizability, from Eq. (A1), is

$$\boldsymbol{\alpha}_\sigma'^{-1} = \frac{1}{\epsilon_0 V_\sigma}\left[\mathbf{L}_\sigma + \begin{pmatrix} -\omega^2 & i\omega\omega_c & 0 \\ -i\omega\omega_c & -\omega^2 & 0 \\ 0 & 0 & -\omega^2 \end{pmatrix}\frac{1}{\omega_p^2}\right], \tag{7}$$

in which we are assuming the lossless model, with $\gamma = 0$. Symbols are defined under Eq. (A1). Also, the quasistatic dipolar Green's function, from Eq. (A4), is

$$\mathbf{G}'_{k\sigma\sigma'} \equiv \lim_{k_0\to 0}\mathbf{G}_{k\sigma\sigma'} = \frac{1}{4\pi\epsilon_0}\sum_{m\neq 0}\mathbf{C}_{\sigma\sigma'}(m)\frac{e^{ikmd}}{r^3_{0m\sigma\sigma'}}, \tag{8}$$

where for the case shown in Fig. 1, relative position vectors $\mathbf{r}_{0m\sigma\sigma'}$ are defined by Eq. (A6), and

$$\mathbf{C}_{AA}(m) = \mathbf{C}_{BB}(m) = \begin{pmatrix} 2 & 0 & 0 \\ 0 & -1 & 0 \\ 0 & 0 & -1 \end{pmatrix}, \tag{9a}$$

$$\mathbf{C}_{AB}(m) = \begin{pmatrix} \frac{3m^2d^2}{m^2d^2+t_y^2} - 1 & \frac{3mdt_y}{m^2d^2+t_y^2} & 0 \\ \frac{3mdt_y}{m^2d^2+t_y^2} & \frac{3t_y^2}{m^2d^2+t_y^2} - 1 & 0 \\ 0 & 0 & -1 \end{pmatrix}, \tag{9b}$$

$$\mathbf{C}_{BA}(m) = \mathbf{C}_{AB}(-m). \tag{9c}$$

The above was obtained by putting Eq. (A6) into (A5) in Appendix A 3. Some properties of $\mathbf{G}'_{k\sigma\sigma'}$ are discussed in Appendix A 4.

B. $\mathcal{T}$ and $\mathcal{RT}$ transformation on the system

When $\mathcal{T}$ operates on the system, it turns k into $-k$ and takes a complex conjugate (see also Appendix A 5):

$$\mathcal{T}\mathbf{M}_k(\omega)\mathcal{T}^{-1} = \mathbf{M}_{-k}(\omega)^*. \tag{10}$$

In the quasistatic limit, Eq. (10) can be written as

$$\mathcal{T}\left(\boldsymbol{\alpha}_\sigma'^{-1} - \mathbf{G}'_{k\sigma\sigma'}\right)\mathcal{T}^{-1} = \left(\boldsymbol{\alpha}_\sigma'^{-1}\right)^* - \mathbf{G}'_{k\sigma\sigma'}. \tag{11}$$

Therefore, $\mathcal{T}\mathbf{M}_k(\omega)\mathcal{T}^{-1} = \mathbf{M}_k(\omega)$ only if $(\boldsymbol{\alpha}_\sigma'^{-1})^* = \boldsymbol{\alpha}_\sigma'^{-1}$, which means $\omega_c = 0$. That is, the system has $\mathcal{T}$ symmetry if external $\mathbf{B} = 0$.

For the $\mathcal{RT}$ transformation, first we notice that $\mathcal{R}^{-1} = \mathcal{R}$, then $(\mathcal{RT})\mathbf{M}_k(\omega)\mathcal{RT}^{-1} = \mathcal{RT}\mathbf{M}_k(\omega)\mathcal{TR}$. In the quasistatic limit for the case shown in Fig. 1, with Eq. (10), we have

$$\begin{aligned}&\mathcal{RT}\boldsymbol{\alpha}_\sigma'^{-1}\delta_{\sigma\sigma'}\mathcal{TR} \\ &= \begin{bmatrix} 0 & \mathbf{R} \\ \mathbf{R} & 0 \end{bmatrix}\begin{bmatrix} \boldsymbol{\alpha}_A'^{-1*} & 0 \\ 0 & \boldsymbol{\alpha}_B'^{-1*} \end{bmatrix}\begin{bmatrix} 0 & \mathbf{R} \\ \mathbf{R} & 0 \end{bmatrix} \\ &= \begin{bmatrix} \boldsymbol{\alpha}_B'^{-1} & 0 \\ 0 & \boldsymbol{\alpha}_A'^{-1} \end{bmatrix}.\end{aligned} \tag{12a}$$

Similarly,

$$\mathcal{RT}\mathbf{G}'_{k\sigma\sigma'}\mathcal{TR} = \mathbf{G}'_{k\sigma\sigma'}. \tag{12b}$$

Equation (12) implies that the $\mathcal{RT}$ transformed system is not generally identical to the nontransformed one. So the chain in Fig. 1 has $\mathcal{RT}$ symmetry only if $\boldsymbol{\alpha}'_A = \boldsymbol{\alpha}'_B$, which is not true.

The dispersion relation can be obtained by solving determinant equation $\det[\mathbf{M}_k(\omega)] = 0$. Neglecting z components, Appendix A 4 shows that it is a polynomial with $G'_{kAB,xy}$ up to second order, and $G'_{kAB,xy}$ is the only term which is odd in k in the determinant polynomial. Nonreciprocal dispersion only comes out when the polynomial is not an even function of k, which means the coefficient of $G'_{kAB,xy}$, given by

$$\frac{-2i\omega\omega_c}{\omega_p^2\epsilon_0}\left(\frac{1}{V_A} - \frac{1}{V_B}\right)(G'_{kAA,xx}G'_{kAB,yy} - G'_{kAA,yy}G'_{kAB,xx}),$$

is nonzero. It is the case that both $\omega_c \neq 0$ and $V_A \neq V_B$; that is, external magnetic field $\mathbf{B} \neq 0$ and the particles A and B are not identical. Therefore, $\mathcal{T}$ and $\mathcal{RT}$ symmetry should not be present in our case of Fig. 1.

V. ONE-WAY WAVE PROPAGATION AND ENERGY TRANSMISSION

The nonreciprocal bands in Fig. 2(a), subpanel (ii), predict that only guided modes with positive group velocities are allowed within the range $\Delta\omega$, which gives one-way propagation behavior. We demonstrate the propagation behavior and energy transmission of the magnetized diatomic chain by considering its finite version in this section.

A. One-way wave propagation

For a finite magnetized diatomic chain system containing N unit cells, Eq. (1) can be written in a matrix equation form $\mathbf{M}(\omega)\mathbf{p} = \mathbf{E}^{\text{ext}}$, where $\mathbf{M}(\omega)$ is a $(12N+6)\times(12N+6)$ square matrix vectorized from $\mathbf{M}_{nm\sigma\sigma'} = \boldsymbol{\alpha}_\sigma^{-1}(\omega)\delta_{nm}\delta_{\sigma\sigma'} - \mathbf{G}_{nm\sigma\sigma'}$. $\mathbf{p}$ and $\mathbf{E}^{\text{ext}}$ are column vectors vectorized from $\mathbf{p}_{m;\sigma'}$ and $\mathbf{E}^{\text{ext}}_{n;\sigma}$, where each has $(2N+1)\times 2\times 3 = 12N+6$ elements ($2N+1$ unit cells, 2 atoms per unit cell, and 3 spatial dimensions in our system). Since $\mathbf{M}(\omega)$ is known, and $\mathbf{E}^{\text{ext}}$ depends on our choices, the excited dipole moments $\mathbf{p}$ can be found by evaluating the inverse:

$$\mathbf{p} = \mathbf{M}(\omega)^{-1}\mathbf{E}^{\text{ext}}. \tag{13}$$

We study the finite version of magnetized diatomic chain in Fig. 2(a), with $N = 46$ and plasma collision frequency $\gamma = 0$. Two types of driving polarizations are applied only to the site $n = 0$, coherent in the x direction, or coherent in the y direction; see Fig. 4(b), subpanels (i) and (ii). In both cases, $\mathbf{E}^{\text{ext}}_{n;\sigma} = 0$ for $n \neq 0$, while $\mathbf{E}^{\text{ext}}_{0;A} = \mathbf{E}^{\text{ext}}_{0;B} = (1,0,0)^{\text{T}}$ for case (i), and $\mathbf{E}^{\text{ext}}_{0;A} = \mathbf{E}^{\text{ext}}_{0;B} = (0,1,0)^{\text{T}}$ for case (ii).

The norm of excited dipole moments by three driving frequencies is shown in Fig. 4(a). Subpanels (1) and (2) correspond to coherent driving in the x direction and y direction. From Fig. 4(a), we see the system supports two-way propagation at $\omega = 0.555\omega_p$, as there are excitations throughout the chain; and supports one-way propagation at $\omega = 0.546\omega_p$, as only spheres on the right are excited; and no supported modes at $\omega = 0.538\omega_p$, as there is no excitation on both sides. This is reasonable, as the slope of the dispersion relation is the group velocity of the coupled plasmon mode. From Fig. 2(a), we see that at $\omega = 0.546\omega_p$, only the mode with positive k is allowed, and therefore only the mode with $+x$ propagation is supported at this frequency. Note that reversing the propagation direction can be easily done by just flipping

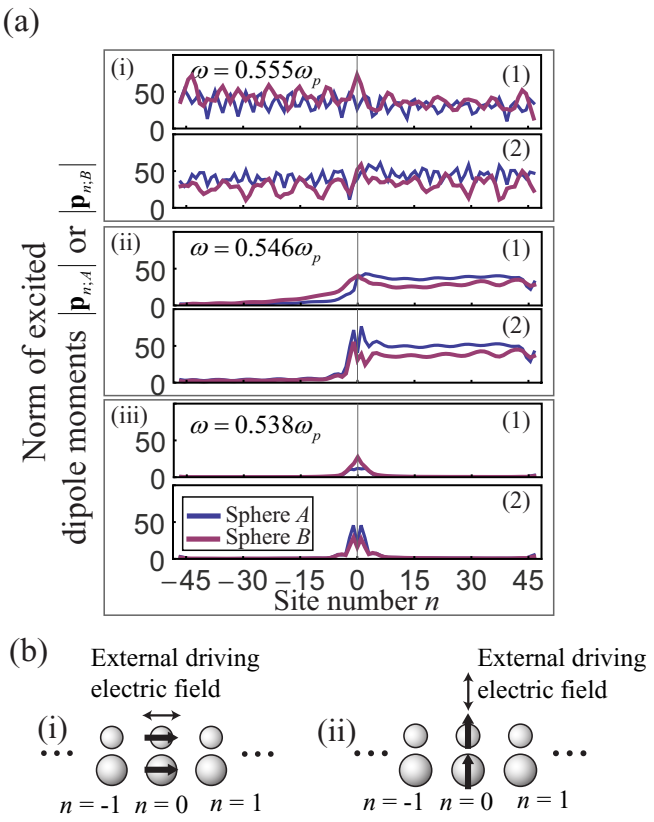

FIG. 4. (Color online) (a) Dipole moments excited on a finite magnetized diatomic chain system (93 cells). An external driving electric field is applied to the middle of the chain ($n = 0$) with driving frequency (i) $\omega = 0.555\omega_p$, (ii) $0.546\omega_p$, (iii) $0.538\omega_p$, indicated by dotted lines in Fig. 2(a). The subpanels in each frequency correspond to two types of driving polarization, coherent in the x or y direction, labeled by (1) and (2). Note that at $\omega = 0.546\omega_p$, one-way propagation occurred, as only modes with positive k are allowed. (b) External driving electric polarization. (i) Coherent in x direction; (ii) coherent in y direction.

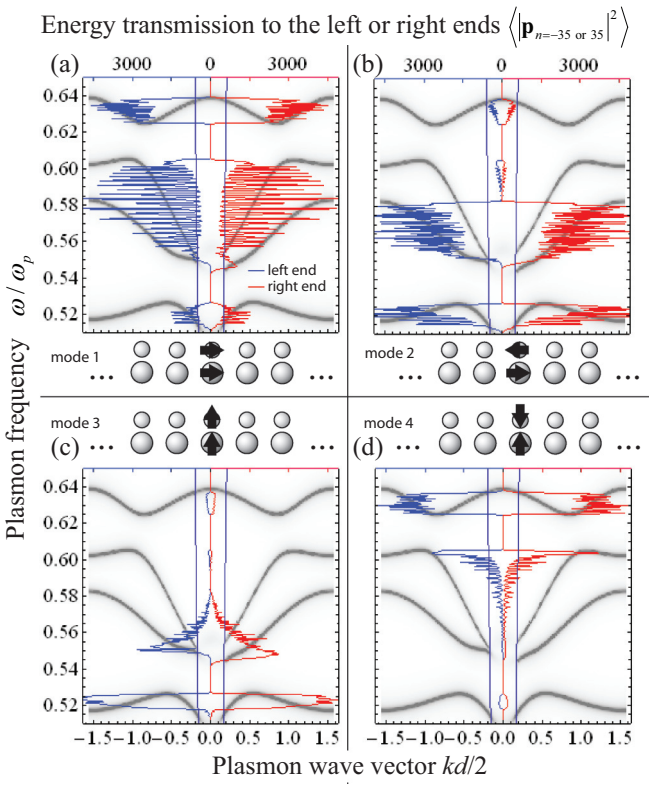

FIG. 5. (Color online) Energy transmissions to the left end ($n = -35$) or the right end ($n = 35$). Energy density is proportional to the quantity $\langle|\mathbf{p}_n|^2\rangle$ (defined in text), and is plotted in the figure. Left (right) end quantity is denoted by the blue (red) curve and uses the left (right) upper horizontal frame ticks. The magnetized diatomic chain dispersion relation is drawn as a background for reference. Panels (a)–(d) correspond to different external driving polarizations, which are pictured in the subpanels (modes 1–4). One-way propagation property is demonstrated at $\omega \sim 0.546\omega_p$, where red curve is finite but blue curve is zero. A little material damping $\gamma = 0.0004\omega_p$ is added to the nanoparticles here, which is to reduce extreme fluctuations so that excitations can be seen more clearly.

the direction of the external static magnetic field; this gives us a switchable optical isolator.

B. One-way energy transmission

Energy transmission is usually hard to define in plasmonic waveguides. Here we infer the transmission of the diatomic chain shown in Fig. 1 by reading the dipole moments $\mathbf{p}_{n;\sigma}$ excited on nanoparticles. Since energy density is proportional to the square of electric field $|\mathrm{Re}(\mathbf{E})|^2$, and since dipole moment satisfies $\mathbf{p} = \boldsymbol{\alpha}\mathbf{E}$, the time-averaged energy density of a particle σ at cell n is thus proportional to $|\mathbf{p}_{n;\sigma}|^2 \equiv \mathbf{p}_{n;\sigma} \cdot \mathbf{p}^*_{n;\sigma}$, which gives the sense of energy transmission. We consider the quantity defined by

$$\langle|\mathbf{p}_n|^2\rangle = \frac{1}{9}\sum_{m=n-4}^{n+4}(|\mathbf{p}_{m;A}|^2 + |\mathbf{p}_{m;B}|^2).$$

In the above we picked 4 cells near the nth for spatial average. One can improve by picking more cells, but in that case the chain has to be longer, or this is no longer a local quantity at cell n. This quantity is displayed in Fig. 5. There are 4 driving polarization modes to excite the system, two in phase and two out of phase [26], denoted by modes 1 to 4 as shown in the subpanels of Fig. 5. It shows that there is no energy transmission within band gaps, since $\langle|\mathbf{p}_{35}|^2\rangle = \langle|\mathbf{p}_{-35}|^2\rangle = 0$ at $\omega \sim 0.54\omega_p$ and $\omega \sim 0.61\omega_p$. The one-way property can be seen at $\omega = 0.546\omega_p$ in Figs. 5(a)–5(c), in which the red curve is finite while the blue curve is zero, implying that there is energy transmission to the right end but no transmission to the left end.

From Fig. 5 we also see that different modes excite different frequency ranges. Polarization modes 1 to 4 correspond to $\omega > 0.55\omega_p$, $\omega < 0.58\omega_p$, $\omega < 0.56\omega_p$, and $\omega > 0.62\omega_p$, respectively. This can be explained by using the band hybridization model (discussed in the next section), which is shown in Fig. 2(a), subpanel (ii).

C. One-way region dispersion and propagation length

In this subsection, we discuss the properties near the one-way region of Fig. 2(a), subpanel (ii), in more detail and

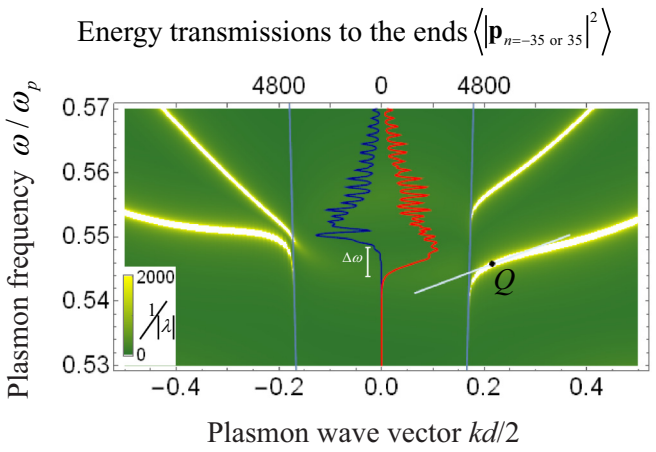

FIG. 6. (Color online) Higher resolution of the density plot for the one-way region shown in Fig. 2(a), subpanel (ii). The brightness of a point reflects the electric response of the structure, which indicates how "easily" a mode can be excited. The two solid light blue lines are light lines. The blue and the red solid lines are the left and right energy transmissions excited by mode 3, which is a higher resolution version of Fig. 5(c). The horizontal dashed line represents $\omega/\omega_p = 0.546$, which cuts the dispersion at point Q and the tail on the left. The modes at the tail are difficult to excite; therefore a mode with positive group velocity (positive slope, indicated by the short solid white line) results. Range of one-way frequency $\Delta\omega$ can also be estimated by reading the transmission at which approximately left transmission is zero while right transmission is finite.

estimate the propagation length of the one-way mode in the presence of material absorptive losses. The high-resolution plot near this one-way region is shown in Fig. 6 with bright narrow lines indicating the plasmon modes. In the figure, the brightness reflects the strength of the mode. The nearly vertical tails of the dispersion bands near the light lines are the results from interacting with the free photons [15,27]. It should be noted that the tails of bands which align very much with the light line are hard to excite because of their tiny residues of poles [27,28]. In Fig. 6, it is also shown that the quasimodes inside the light cone are so poor in mode quality (as indicated by the spreading of brightness in the density plot). As a result, near the one-way region, only one mode of the well-defined propagation direction can be effectively excited by a localized source. For reference, higher resolution of transmission by excitation mode 3 is also shown in Fig. 6 (the solid blue and red lines). The range for the one-way frequency $\Delta\omega \sim 0.005\omega_p$ (also marked in Fig. 6) is estimated from the strong asymmetric transmission region where the amount of dipole moments propagating to the right is much higher than that to the left.

To estimate the propagation length of the one-way mode (point Q in Fig. 6) in the presence of material absorptive losses, we follow the method in Ref. [29]. We consider plasma collision frequency $\gamma = 0.002\omega_p$ in the Drude model, which is appropriate for silver. By putting $kd = 0.216$ to the equation $\det\mathbf{M}_k(\omega) = 0$, the complex root is found to be $\omega/\omega_p = 0.546 - 0.000963i$, where the inverse of the imaginary part is the lifetime of the plasmon mode and the propagation length can be estimated by multiplying the lifetime by the group velocity $d\omega/dk \sim 0.015\omega_p d$ [slope at $Q = d(\omega/\omega_p)/d(kd/2) \sim 0.03$]. As a result, the propagation length $= \frac{1}{0.000963\omega_p} \times \frac{d\omega}{dk} = 15.6d$.

VI. HYBRIDIZATION OF BANDS IN DIATOMIC CHAIN

There are four surface plasmon resonant modes for isolated dimer particles, two transverse modes (in-phase and antiphase oscillations) and two longitudinal modes [30]. The four modes form dispersion bands when the dimer particles are duplicated, becoming a diatomic chain. After that, the dispersion relation of the magnetized diatomic chain can be understood as a result of four-band hybridization, colored in blue, yellow, red, and green in Fig. 2(a), subpanel (ii). We can see the transition of the four bands in Fig. 7.

For better understanding of the hybridization, here we consider the diatomic chain formed by ellipsoids. Spheres in Fig. 1 are replaced by ellipsoids with varying a_x^σ and a_y^σ, where $t_y = 0.75d$. Figure 7(a), subpanels (i)–(iv), show the dispersion relations with increasing a_y^σ. In these 4 cases, $a_x^A = 0.35d$, $V_B/V_A = 0.5$, and $\mathbf{B} = 0$. Corresponding unit cell structures are depicted in Fig. 7(b), subpanels (i) to (iv). Figure 7(a), subpanel (i), shows four separated bands. The lower two bands move up and cross the upper two bands when the particles are more spherical, as shown in subpanels (i)–(iv). If one further applies external static magnetic field to case (iv) such that $\omega_c = 0.005\omega_p$, we have case (v), which is the case

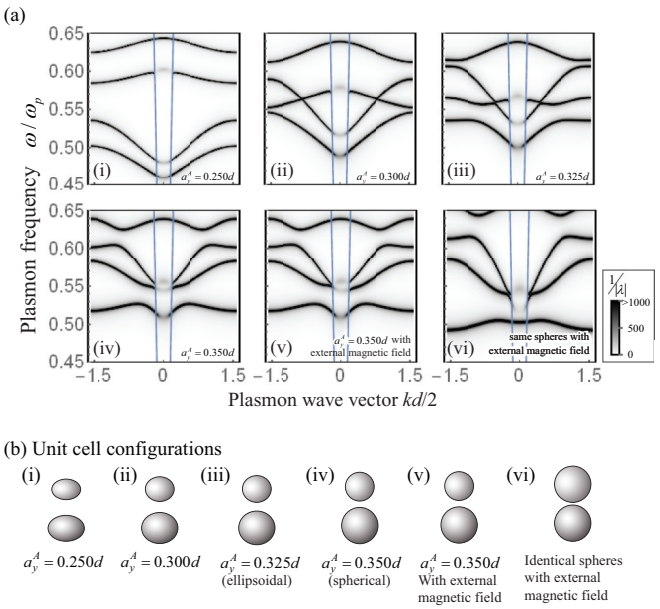

FIG. 7. (Color online) (a) Dispersion relations of diatomic chains formed by different ellipsoids. Corresponding unit cell configurations are shown in (b). Moving from (i) to (vi), semiminor axes a_y^σ are increased one by one, so nanoparticles become more and more spherical. $\mathbf{B} = 0$, $a_x^A = 0.35d$, and $V_B/V_A = 0.5$ in (i) to (vi). From (i) to (vi), the lower two bands move upwards, cross the upper two bands, and hybridize each other. Note that (iv) is the case that A and B are spherical. (v) is different from (iv) by adding external static magnetic field ($\omega_c = 0.005\omega_p$), resulting in a nonreciprocal dispersion. In (vi), A and B are identical spheres with $a_x^A = a_x^B = 0.35d$. Although $\mathbf{B} \neq 0$, the dispersion is reciprocal as it is protected by $\mathcal{P}$ symmetry.

in Fig. 2(a). Thus, in cases (i)–(v), we see the deformation of bands, and so conclude that the dispersion in case (iv) of Fig. 7 is formed by hybridization of the four bands. Figure 7(b), subpanel (vi), shows the case where nanoparticle B is identical to nanoparticle A; that is, $a_x^\sigma = a_y^\sigma = 0.35d$, where $\sigma = A$ or B. This is obtained by replacing all particles B by A in Fig. 7(b), subpanel (v). The bands in Fig. 7(b), subpanel (vi), are symmetric, as it has both $\mathcal{RT}$ and $\mathcal{P}$ symmetry. From these we know the exitance of $\mathbf{B}$ and nonidentical spheres are essential to achieve nonreciprocal bands.

The hybridization model also explains the excitations in Fig. 5. Figure 2(a), subpanel (ii), shows that the upper two bands contain parts that are original from the red dashed band, and therefore the excitation by polarization mode 1 is prominent at the upper two bands, as found in Fig. 5(a). This is because the oscillation mode of the red dashed band at $k = 0$ is the same as mode 1. Similarly, the lower two bands contain parts that are original from the green dashed band, and hence excitation by polarization mode 2 is prominent at the lower two bands.

VII. CONCLUSIONS

To conclude, we used a compact nonchiral magnetized plasmonic chain to demonstrate the crucial role of $\mathcal{RT}$ symmetry in the design of these subwavelength waveguides with nonreciprocal dispersion $[\omega(-k) \neq \omega(k)]$. The hybridization among four plasmon modes and free-photon modes gives rise to a frequency range where only guided modes in one direction are allowed. While we are considering a weaker magnetic field, this operation frequency range is already much wider than that in Ref. [10]. Matrix representations of the symmetry operators were used to explain explicitly how the spectral reciprocity is protected by $\mathcal{T}$, $\mathcal{P}$, and $\mathcal{RT}$ symmetries. The results may provide a clear guidance on the design of one-way waveguides. After the review process of our article, we became aware of another article considering only spatial symmetries of similar physical systems [31].

ACKNOWLEDGMENTS

This work was supported by the Hong Kong Research Grant Council through the Area of Excellence Scheme (Grant No. AoE/P-02/12), the Hong Kong Polytechnic University under Grant No. G-YBCH, and the National Natural Science Foundation of China under Grant No. 11204036. We thank Prof. C. T. Chan and Dr. S. W. Shu for useful discussions.

APPENDIX

1. Polarizability and Drude model in external B

The inverse polarizability of an ellipsoidal particle σ ($a_x^\sigma \geqslant a_y^\sigma = a_z^\sigma$) is given by [10,32,33]

$$\boldsymbol{\alpha}_\sigma^{-1} = \frac{1}{\epsilon_0 V}\left[\left(\frac{\boldsymbol{\epsilon}(\omega)}{\epsilon_0} - \mathbf{I}\right)^{-1} + \mathbf{L}_\sigma\right] - \frac{ik_0^3}{6\pi\epsilon_0}\mathbf{I}, \tag{A1}$$

where volume $V_\sigma \equiv 4\pi a_x^\sigma a_y^\sigma a_z^\sigma/3$, $\mathbf{I}$ is identity 3×3 matrix, k_0 is light wave vector in free space, and parameter $\mathbf{L}_\sigma$ depends on the particle's shape, which is given by $\mathbf{L}_\sigma = \mathrm{diag}(N_x, N_y, N_z)$. For spherical particles, $N_x = N_y = N_z = 1/3$. For ellipsoidal particles, $N_x = (1+e^2)[\ln\frac{1+e}{1-e} - 2e]/(2e^3)$ and $N_y = N_z = (1-N_x)/2$, where $e = \sqrt{1 - a_y^{\sigma\,2}/a_x^{\sigma\,2}}$. As we consider nanoparticles A and B are of the same shape in this paper, so $\mathbf{L}_A = \mathbf{L}_B$. The last term with k_0^3 accounts for the radiation correction [34], which will vanish in the quasistatic approximation.

With the Drude model, the dielectric tensor is in the form [17,35]

$$\frac{\boldsymbol{\epsilon}(\omega)}{\epsilon_0} = \begin{pmatrix} \epsilon_{xx} & \epsilon_{xy} & 0 \\ -\epsilon_{xy} & \epsilon_{yy} & 0 \\ 0 & 0 & \epsilon_{zz} \end{pmatrix}, \tag{A2}$$

in which $\epsilon_{xx} = \epsilon_{yy} = 1 - \omega_p^2(\omega + i\gamma)/[\omega(\omega+i\gamma)^2 - \omega\omega_c^2)]$, $\epsilon_{xy} = -i\omega_p^2\omega_c/[\omega(\omega+i\gamma)^2 - \omega\omega_c^2]$, $\epsilon_{zz} = 1 - \omega_p^2/(\omega^2 + i\gamma\omega)$. γ, ω_p, and ω_c are plasma collision frequency, plasmon frequency, and cyclotron frequency. In the case without material loss, $\lambda = 0$, and $\boldsymbol{\epsilon}(\omega)$ becomes real. More terms have to be added to the static polarizability if one wants an accurate numerical evaluation on lossy materials, but it is not of interest in this paper. Further discussions can be found in Chap. 8 of Ref. [35].

2. Coupled dipole equation in k space

In Eq. (1), defining $\mathbf{M}_{nm\sigma\sigma'} = \boldsymbol{\alpha}_\sigma^{-1}\delta_{nm}\delta_{\sigma\sigma'} - \mathbf{G}_{nm\sigma\sigma'}$, putting $\mathbf{p}_{m;\sigma'} = \mathbf{p}_{k;\sigma'}e^{ikmd}$, and in the case $\mathbf{E}_{n;\sigma}^{\mathrm{ext}} = 0$, we have

$$\sum_{\sigma'}\left(\sum_m \mathbf{M}_{nm\sigma\sigma'}e^{ikmd}\right)\mathbf{p}_{k;\sigma'} = 0.$$

Multiplying both sides by e^{-iknd}, and noticing that $\mathbf{M}_{nm\sigma\sigma'}$ depends on $m-n$ only, we have $\mathbf{M}_{nm\sigma\sigma'} = \mathbf{M}_{0,m-n,\sigma\sigma'}$, and thus

$$\sum_{\sigma'}\left(\sum_m \mathbf{M}_{0,m-n,\sigma\sigma'}e^{ik(m-n)d}\right)\mathbf{p}_{k;\sigma'} = 0.$$

As the sum m runs from $-\infty$ to ∞, we have

$$\sum_{\sigma'}\left(\sum_m \mathbf{M}_{0m\sigma\sigma'}e^{ikmd}\right)\mathbf{p}_{k;\sigma'} = 0.$$

Writing it in matrix form, we have

$$\sum_m \left\{\begin{bmatrix} \boldsymbol{\alpha}_A^{-1} & 0 \\ 0 & \boldsymbol{\alpha}_B^{-1} \end{bmatrix}\delta_{0m} - \begin{bmatrix} \mathbf{G}_{0mAA} & \mathbf{G}_{0mAB} \\ \mathbf{G}_{0mBA} & \mathbf{G}_{0mBB} \end{bmatrix}e^{ikmd}\right\}\begin{bmatrix} \mathbf{p}_{k;A} \\ \mathbf{p}_{k;B} \end{bmatrix} = 0. \tag{A3}$$

This gives Eq. (2).

3. Dynamic dipolar Green's function for diatomic chain system

The dipolar coupling between the particle σ' in the mth cell and the particle σ in the nth cell depends on $m-n$ only, i.e., $\mathbf{G}_{nm\sigma\sigma'} = \mathbf{G}_{0,m-n,\sigma\sigma'}$, so we only show elements $\mathbf{G}_{0m\sigma\sigma'}$ here. Also, the position vector of the particle σ' in the mth cell is denoted by $\mathbf{r}_{m\sigma'}$. The relative position vector is then $\mathbf{r}_{0m\sigma\sigma'} \equiv \mathbf{r}_{0\sigma} - \mathbf{r}_{m\sigma'}$, and the corresponding unit vector is therefore $\boldsymbol{\rho}_{\sigma\sigma'}(m) \equiv \mathbf{r}_{0m\sigma\sigma'}/r_{0m\sigma\sigma'}$. Spatial components of the

unit vector are denoted by $\rho_{\sigma\sigma'}(m)_x$, $\rho_{\sigma\sigma'}(m)_y$, and $\rho_{\sigma\sigma'}(m)_z$. The dynamic coupling is well known and is given by [10]

$$\mathbf{G}_{0m\sigma\sigma'} = \frac{e^{ik_0 r_{0m\sigma\sigma'}}}{4\pi\epsilon_0} \times \left[\mathbf{A}_{\sigma\sigma'}(m) \frac{k_0^2}{r_{0m\sigma\sigma'}} + \mathbf{C}_{\sigma\sigma'}(m) \left(\frac{1}{r_{0m\sigma\sigma'}^3} - \frac{ik_0}{r_{0m\sigma\sigma'}^2} \right) \right] \tag{A4}$$

for $m \neq 0$ together with $\sigma' \neq \sigma$; otherwise $\mathbf{G}_{00\sigma\sigma} = 0$, as a particle is not interacting itself by generating electric field. In the above, ϵ_0 is free-space permittivity, and $k_0 = \omega/c$ is the light wave vector in free space. Matrices in the above are

$$\mathbf{A}_{\sigma\sigma'}(m) = \begin{pmatrix} \rho_{\sigma\sigma'}(m)_y^2 & -\rho_{\sigma\sigma'}(m)_y \rho_{\sigma\sigma'}(m)_x & 0 \\ -\rho_{\sigma\sigma'}(m)_x \rho_{\sigma\sigma'}(m)_y & \rho_{\sigma\sigma'}(m)_x^2 & 0 \\ 0 & 0 & 1 \end{pmatrix}$$

and

$$\mathbf{C}_{\sigma\sigma'}(m) = \begin{pmatrix} 3\rho_{\sigma\sigma'}(m)_x^2 - 1 & 3\rho_{\sigma\sigma'}(m)_x \rho_{\sigma\sigma'}(m)_y & 0 \\ 3\rho_{\sigma\sigma'}(m)_y \rho_{\sigma\sigma'}(m)_x & 3\rho_{\sigma\sigma'}(m)_y^2 - 1 & 0 \\ 0 & 0 & -1 \end{pmatrix}. \tag{A5}$$

For the system shown in Fig. 1 or Fig. 2(a), subpanel (i), relative position vectors are

$$\begin{aligned} \mathbf{r}_{0mAA} &= \mathbf{r}_{0mBB} = (-md,0,0)^{\mathrm{T}}, \\ \mathbf{r}_{0mAB} &= (-md,-t_y,0)^{\mathrm{T}}, \\ \mathbf{r}_{0mBA} &= (-md,t_y,0)^{\mathrm{T}}. \end{aligned} \tag{A6}$$

For the system shown in Fig. 2(b), subpanel (i), relative position vectors are

$$\begin{aligned} \mathbf{r}_{0mAA} &= \mathbf{r}_{0mBB} = (-md,0,0)^{\mathrm{T}}, \\ \mathbf{r}_{0mAB} &= (-md - t_x,0,0)^{\mathrm{T}}, \\ \mathbf{r}_{0mBA} &= (-md + t_x,0,0)^{\mathrm{T}}. \end{aligned} \tag{A7}$$

4. Properties of quasistatic Green's function $\mathbf{G}'_{k\sigma\sigma'}$ for system in Fig. 2(a)

There are some properties about the matrix $\mathbf{G}'_{k\sigma\sigma'}$ regarding to the system in Fig. 1. From Eq. (8), one can see

$$\mathbf{G}'^{*}_{-k\sigma\sigma'} = \mathbf{G}'_{k\sigma\sigma'}. \tag{A8}$$

Also, from Eq. (9a) we know that $\mathbf{G}'_{kAA} = \mathbf{G}'_{kBB}$, and they are both diagonal, so we have

$$\begin{aligned} \mathbf{R}\mathbf{G}'_{kAA}\mathbf{R}^{-1} &= \mathbf{G}'_{kAA} = \mathbf{G}'_{kBB}, \\ \mathbf{R}\mathbf{G}'_{kBB}\mathbf{R}^{-1} &= \mathbf{G}'_{kBB} = \mathbf{G}'_{kAA}, \end{aligned} \tag{A9a}$$

where $\mathbf{R} = \mathrm{diag}(1,-1,-1)$ is the rotation matrix about the x axis with 180°. Furthermore, Eq. (9c) tells us that off-diagonal elements in $\mathbf{G}'_{kAB}$ and $\mathbf{G}'_{kBA}$ are purely imaginary, and Eq. (9b) implies $\mathbf{G}^{*}_{kAB} = \mathbf{G}_{kBA}$, so we have

$$\begin{aligned} \mathbf{R}\mathbf{G}'_{kAB}\mathbf{R}^{-1} &= \mathbf{G}'^{*}_{kAB} = \mathbf{G}'_{kBA}, \\ \mathbf{R}\mathbf{G}'_{kBA}\mathbf{R}^{-1} &= \mathbf{G}'^{*}_{kBA} = \mathbf{G}'_{kAB}. \end{aligned} \tag{A9b}$$

With Eqs. (A8) and (A9), we have Eq. (12b).

Elements in $\mathbf{G}'_{k\sigma\sigma'}$ are functions of k. By expanding the terms and Eq. (A9), we see that $\mathbf{G}'_{kAA}$, $G'_{kAB,xx}$, and $G'_{kAB,yy}$ are purely real and even in k, while $G'_{kAB,xy}$ is purely imaginary and odd in k. Hence, we deduced that, neglecting z components,

$$\begin{aligned} \mathbf{G}'_{kAA} = \mathbf{G}'_{kBB} &= \begin{pmatrix} G'_{kAA,xx} & 0 \\ 0 & G'_{kAA,yy} \end{pmatrix}, \\ \mathbf{G}'_{kAB} &= \begin{pmatrix} G'_{kAB,xx} & G'_{kAB,xy} \\ G'_{kAB,xy} & G'_{kAB,yy} \end{pmatrix}, \\ \mathbf{G}'_{kBA} &= \begin{pmatrix} G'_{kAB,xx} & -G'_{kAB,xy} \\ -G'_{kAB,xy} & G'_{kAB,yy} \end{pmatrix}. \end{aligned}$$

Therefore, the determinant

$$|\mathbf{M}_k(\omega)| = \begin{vmatrix} \boldsymbol{\alpha}'^{-1}_{A}(\omega) - \mathbf{G}'_{kAA} & -\mathbf{G}'_{kAB} \\ -\mathbf{G}'_{kBA} & \boldsymbol{\alpha}'^{-1}_{B}(\omega) - \mathbf{G}'_{kAA} \end{vmatrix}$$

is a polynomial with $G'_{kAB,xy}$ up to second order.

5. The $\mathcal{T}$ operator

Regarding Eq. (4), noticing $\mathcal{T}^{-1} = \mathcal{T}$, we have

$$\begin{aligned} \sum_m \mathcal{T}^{-1}\mathbf{M}_{nm}\mathcal{T}\mathbf{p}_m &= \sum_m \mathcal{T}\mathbf{M}_{nm}\mathcal{T}\mathbf{p}_k e^{ikmd} \\ &= \mathcal{T}\sum_m \mathbf{M}_{nm}\mathbf{p}_k^{*} e^{-ikmd} \\ &= \mathcal{T}e^{-iknd}\sum_m e^{iknd}\mathbf{M}_{nm}\mathbf{p}_k^{*} e^{-ikmd} \\ &= \mathcal{T}\sum_m \mathbf{M}_{nm}e^{-ik(m-n)d}\mathbf{p}_k^{*} e^{-iknd} \\ &= \mathcal{T}\mathbf{M}_{-k}\mathbf{p}_k^{*} e^{-iknd} = \mathbf{M}_{-k}^{*}\mathbf{p}_k e^{iknd}. \end{aligned}$$

In the above, we used the fact that $\mathbf{M}_{nm} = \mathbf{M}_{0,m-n}$ and defined $\mathbf{M}_k = \sum_m \mathbf{M}_{0m}e^{ikmd}$. The last line proves Eq. (10).

6. The $\mathcal{RT}$ operator on diatomic chain system in Fig. 2(b)

The double chain in Fig. 2(b) has $\mathcal{RT}$ symmetry. Here we show that $\mathbf{M}_k(\omega)$ commutes with $\mathcal{RT}$ in the quasistatic limit. By Eqs. (6b) and (11),

$$\begin{aligned} &(\mathcal{RT})\boldsymbol{\alpha}'^{-1}_{\sigma}\delta_{\sigma\sigma'}(\mathcal{RT})^{-1} \\ &= \begin{bmatrix} \mathbf{R} & 0 \\ 0 & \mathbf{R} \end{bmatrix}\mathcal{T}\begin{bmatrix} \boldsymbol{\alpha}'^{-1}_{A} & 0 \\ 0 & \boldsymbol{\alpha}'^{-1}_{B} \end{bmatrix}\mathcal{T}\begin{bmatrix} \mathbf{R} & 0 \\ 0 & \mathbf{R} \end{bmatrix} \\ &= \begin{bmatrix} \boldsymbol{\alpha}'^{-1}_{A} & 0 \\ 0 & \boldsymbol{\alpha}'^{-1}_{B} \end{bmatrix} = \boldsymbol{\alpha}'^{-1}_{\sigma}\delta_{\sigma\sigma'}. \end{aligned}$$

Also, by putting Eq. (A7) into (A5), we see $\mathbf{C}_{\sigma\sigma'}(m) = \mathrm{diag}(2,-1,-1)$, and thus $\mathbf{G}'_{k\sigma\sigma'}$ are diagonal. As a result, $\mathbf{R}^{-1}\mathbf{G}_{k\sigma\sigma'}\mathbf{R} = \mathbf{G}_{k\sigma\sigma'}$, and we have

$$(\mathcal{RT})\mathbf{G}_{k\sigma\sigma'}(\mathcal{RT})^{-1} = \mathbf{G}_{k\sigma\sigma'}.$$

7. Comments on π-rotation ($\mathcal{R}$) symmetry and reflection-in-y ($\mathcal{P}_y$) symmetry

We note that for the structure we have considered, the diatomic chain of plasmonic spheres, reflection-in-y followed by time-reverse operation ($\mathcal{P}_y\mathcal{T}$), in which $\mathcal{P}_y$ turns (x,y,z) into $(x,-y,z)$, has the same effects on the chain structure as $\mathcal{RT}$ on the structure. That is, they switch the position atom A and B, but the magnetic field remains unchanged. This operational symmetry has to be avoided in order to have nonreciprocal bands, which means both $\mathcal{P}_y\mathcal{T}$ and $\mathcal{RT}$ symmetry have to be avoided at the same time in order to break the spectral reciprocity. To describe this symmetry, we may refer to it as the result of the $\mathcal{P}_y\mathcal{T}$ symmetry, or the $\mathcal{RT}$ symmetry, but neither operation can be regarded as more fundamental. $\mathcal{RT}$ symmetry is chosen for presentation in our conclusion because we believe rotation is easier to physically visualize, and thus simpler to follow.

[1] J. A. Kong and D. K. Cheng, Proc. IEE **117**, 349 (1970).
[2] C. Altman and A. Schatzberg, Appl. Phys. B **28**, 327 (1982).
[3] R. E. Camley, Surf. Sci. Rep. **7**, 103 (1987).
[4] A. Figotin and I. Vitebsky, Phys. Rev. E **63**, 066609 (2001).
[5] T. Ochiai, Sci. Technol. Adv. Mater. **16**, 014401 (2015).
[6] F. D. M. Haldane and S. Raghu, Phys. Rev. Lett. **100**, 013904 (2008).
[7] K. Fang, Z. Yu, and S. Fan, Phys. Rev. B **84**, 075477 (2011).
[8] Z. Wang, Y. D. Chong, J. D. Joannopoulos, and M. Soljacic, Phys. Rev. Lett. **100**, 013905 (2008).
[9] H. Takeda and S. John, Phys. Rev. A **78**, 023804 (2008).
[10] Y. Hadad and B. Z. Steinberg, Phys. Rev. Lett. **105**, 233904 (2010).
[11] A. Christofi and N. Stefanou, Phys. Rev. B **87**, 115125 (2013).
[12] P.-J. Cheng, C.-H. Tien, and S.-W. Chang, Opt. Express **23**, 10327 (2015).
[13] X. Lin, Y. Xu, B. Zhang, R. Hao, H. Chen, and E. Li, New J. Phys. **15**, 113003 (2013).
[14] W. H. Weber and G. W. Ford, Phys. Rev. B **70**, 125429 (2004).
[15] K. H. Fung and C. T. Chan, Opt. Lett. **32**, 973 (2007).
[16] C. W. Ling, M. J. Zheng, and K. W. Yu, Opt. Commun. **283**, 1945 (2010).
[17] H.-F. Zhang, S.-B. Liu, and X.-K. Kong, Phys. Plasmas **19**, 122103 (2012).
[18] J.-W. Dong and Z.-L. Deng, Opt. Lett. **38**, 2244 (2013).
[19] Where plasma collision frequency $\gamma = 0$.
[20] Y. Hadad, Y. Mazor, and B. Z. Steinberg, Phys. Rev. B **87**, 035130 (2013).
[21] S. M. Wang, T. Li, H. Liu, F. M. Wang, S. N. Zhu, and X. Zhang, Opt. Express **16**, 3560 (2008).
[22] Z. Yu, G. Veronis, Z. Wang, and S. Fan, Phys. Rev. Lett. **100**, 023902 (2008).
[23] C. Altman and K. Suchy, *Reciprocity, Spatial Mapping, and Time Reversal in Electromagnetics* (Springer, New York, 2011), Chap. 7.
[24] J. D. Jackson, *Classical Electrodynamics* (John Wiley and Sons, Inc., Hoboken, NJ, 1999), Chap. 6, 3rd ed.
[25] A. Alu and N. Engheta, Phys. Rev. B **74**, 205436 (2006).
[26] For mode 1, $\mathbf{E}^{\text{ext}}_{0;A} = \mathbf{E}^{\text{ext}}_{0;B} = (1,0,0)^{\text{T}}$; for mode 2, $\mathbf{E}^{\text{ext}}_{0;A} = (1,0,0)^{\text{T}}$ and $\mathbf{E}^{\text{ext}}_{0;B} = (-1,0,0)^{\text{T}}$; for mode 3, $\mathbf{E}^{\text{ext}}_{0;A} = (0,1,0)^{\text{T}}$ and $\mathbf{E}^{\text{ext}}_{0;B} = (0,-1,0)^{\text{T}}$; for mode 4, $\mathbf{E}^{\text{ext}}_{0;A} = (0,1,0)^{\text{T}}$ and $\mathbf{E}^{\text{ext}}_{0;B} = (0,-1,0)^{\text{T}}$.
[27] K. H. Fung, R. C. H. Tang, and C. T. Chan, Opt. Lett. **36**, 2206 (2011).
[28] Y. Hadad and B. Z. Steinberg, Phys. Rev. B **84**, 125402 (2011).
[29] C. Tserkezis, N. Stefanou, G. Gantzounis, and N. Papanikolaou, Phys. Rev. B **84**, 115455 (2011).
[30] V. Myroshnychenko, J. Rodréguez-Fernandez, I. Pastoriza-Santos, A. M. Funston, P. M. Carolina Novo, L. M. Liz-Marzan, and F. J. Garcéa de Abajo, Chem. Soc. Rev. **37**, 1792 (2008).
[31] Y. Mazor, Y. Hadad, and Ben Z. Steinberg, Phys. Rev. B **92**, 125129 (2015).
[32] A. Sihvola, *Electromagnetic Mixing Formulas and Applications* (The Institution of Electrical Engineers, Stevenage, Herts, 1999), Chap. 5.
[33] C. F. Bohren and D. R. Huffman, *Absorption and Scattering of Light by Small Particles* (John Wiley and Sons, Inc., Hoboken, NJ, 1983), Chap. 5.
[34] S. Albaladejo, R. Gomez-Medina, L. S. Froufe-Perez, H. Marincho, R. Carminati, J. F. Torrado, G. Armelles, A. Garcia-Martin, and J. J. Saenz, Opt. Express **18**, 3556 (2010).
[35] F. Capolino, *Theory and Phenomena of Metamaterials* (Taylor and Francis Group, LLC, Boca Raton, FL, 2009), Chap. 8, p. 7.